Improved Photoluminescence Properties of Ternary Terbium Complexes in Mesoporous Molecule Sieves

Suwen Li, Hongwei Song,* Wenlian Li, Xinguang Ren, Shaozhe Lu, Guohui Pan, Libo Fan, Hongquan Yu, Hui Zhang, Ruifei Qin, QiLin Dai, and Tie Wang

Key Laboratory of Excited-State Physics, Changchun Institute of Optics, Fine Mechanics and Physics, Chinese Academy of Sciences, and Graduate School of Chinese Academy of Sciences, 16 Eastern Nan-Hu Road, Changchun 130033, PR China

Received: July 16, 2006; In Final Form: September 8, 2006

Ternary terbium complexes were fully encapsulated and uniformly distributed into the channels of unmodified and modified mesoporous molecule sieves of SBA-15 and characterized by transmission electron micrographs (TEM), Fourier transform infrared spectroscopy (FTIR), ultraviolet−visible (UV−vis) absorption spectra, inductively coupled plasma-atomic emission spectroscopy (ICP-AES), and elemental analysis. The luminescent properties for the encapsulated complexes were systematically studied in contrast to the pure complexes, including excitation and emission spectra, fluorescence dynamics, photostability under UV exposure, and the temperature dependence of intensity and lifetime. The results indicate that the excitation bands assigned to the $\pi-\pi^*$ electron transition of the ligands for Tb complexes encapsulated in SBA-15 were split into different components due to decreased symmetry and disappeared at long wavelengths. Owing to suppressed vibration transitions, the outer quantum efficiency of the $^5D_4$-^7F_J ($J = 0-5$) emissions was enhanced largely in comparison to the pure complexes. In addition, the photostability and thermostability of the emissions were also improved considerably.

Introduction

Rare earth (RE) complexes have been well known to show sharp, intense emission lines upon ultraviolet light irradiation because the effective intramolecular energy transfers from the coordinated ligands to the luminescent central lanthanide ions. Some of the RE complexes demonstrate potential applications in efficient light-conversion molecular devices (LCMDs)[1,2] and organic light-emitting devices (OLEDs).[3−5] However, this kind of materials owns some disadvantages for practical application, such as their low chemical, optical, and thermal stabilities. Recently, because their photophysical properties could be modified by interaction of the host structure, the luminescence properties of RE complexes supported on a solid matrix were studied extensively. For instance, the RE complexes were encapsulated in or adsorbed on host materials, including Langmuir−Blodgett films,[6] sol−gel matrixes,[7,8] zeolites,[9] and silica matrix.[10] Among them, the mesoporous molecular sieves used as a support for RE complexes have attracted particular attention. In the past few years, Xu,[11,12] Zhang,[13] and Gleizes[14] et al. encapsulated different ternary Eu^{3+} complexes into mesoporous channels of MCM-41 via wet impregnation and observed that encapsulation of the ternary Eu^{3+} complexes in MCM-41 gave efficient red emissions. Additionally, Xu et al. observed that in the encapsulated samples Eu^{3+} complexes had better photostability under UV irradiation than the corresponding pure complexes. However, the encapsulation of the ternary Tb^{3+} complexes in mesoporous molecule sieves was reported infrequently.

In this paper, we report the preparation and photoluminescence properties of the RE complexes $Tb(acac)_3phen$ (acac, acetylacetone; phen, 1,10-phenanthroline) encapsulated in mesoporous molecular sieves of SBA-15, which may provide better support for RE complexes because of their larger pore size and better stability[15] in comparison with those of MCM-41. In the preparation, a combined method of press difference and wet impregnation was adopted, which ensured that the RE complexes were effectively filled into the channels of mesoporous molecular sieves. To thoroughly understand the photoluminescence properties of this kind of materials, the spectral properties of this kind of materials were systematically studied. It is interesting to observe that in the pores of SBA-15 the photostability and thermostability of Tb^{3+} ternary complexes were improved considerably. In addition, the outer luminescence efficiency in the encapsulated samples was increased largely over the pure complexes.

Experiments

A. Sample Preparation. Pure $Tb(acac)_3phen$ complexes (labeled with **P**) were synthesized according to ref 16, which had the following molecular structure:

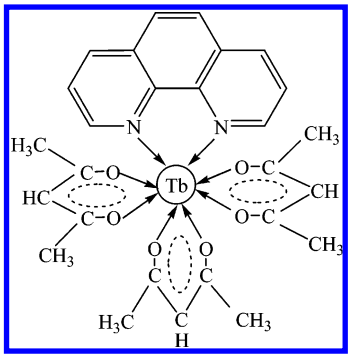

SBA-15 was purchased from Jilin University. The modified SBA-15 was prepared referring to ref 17, with modifier of

* Corresponding author. Address: Key Laboratory of Excited-State Physics, Changchun Institute of Optics, Fine Mechanics and Physics, Chinese Academic of Sciences, 16 Eastern South-Lake Road, Changhcun 130033, P R China. E-mail: hwsong2005@yahoo.com.cn. Fax: 86-431-6176320.

10.1021/jp064509d CCC: $33.50
Published on Web 10/25/2006

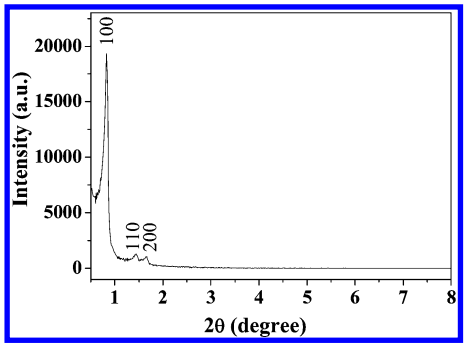

Figure 1. XRD pattern of SBA-15.

3-aminopropyl)triethoxysilane (APTES) (Fluka). The precursor solution was prepared via dissolvation of appropriate amounts of the pure complexes in chloroform solution. Dried SBA-15 (100 mg) was decompressed in a 100 mL round-bottomed flask. When the press was isobaric, the precursor solution was added into the round-bottomed flask slowly; then it was decompressed and placed 24 h in air. The mixture was filtered and washed with acetone until the color (green) of the filtered solution disappeared under the irradiation of a 266-nm laser light. Finally, the resultant products were dried for 2 h in vacuum, which was labeled as sample **A**. The encapsulation method of the Tb(acac)$_3$phen complexes in the modified SBA-15 (labeled as sample **B**) was similar to the method described above.

B. Measurements. The morphologies of the samples were characterized by a JEOL JEM-2010 transmission electron microscope with an accelerating voltage of 200 kV. The FTIR spectra were recorded at a Bio-Rad FTS-3000 (EXCALIBUR SERIES) spectrometer. The UV−vis absorption spectra were recorded at a UV−vis−NIR scanning spectrophotometer (SHIMADZU). The content of the Tb^{3+} ion was analyzed by ICP-AES measurement with a TJA-POEMS spectrometer. The CHN elemental analysis was carried out on a VarioEL analyzer.

Excitation and emission spectra were recorded at room temperature using a Hitachi F-4500 spectrophotometer equipped with a continuous 150 W Xe-arc lamp. The continuous lights separated from a 500 W xenon lamp were used as irradiation, with a line width of 10 nm and a power density of 10−100 μW/cm^2. In the measurements of temperature dependence of emission intensity, the samples were put into a liquid nitrogen cycling system, in which the temperature varied from 77 to 300 K. The 325-nm light came from a He−Cd laser that was used for excitation. The spectra were recorded by a UV-Lab Raman Infinity with a resolution of 2 cm^{-1}. In the measurements of fluorescence dynamics, a 266-nm light generated from the Nd^{3+}:YAG laser combined with a fourth-harmonic-generator was used as pumping, with a repetition frequency of 10 Hz and a duration of 10 ns. The samples were put into a liquid helium cycling system, where the temperature varied from 10 to 300 K. The spectra were recorded by a Spex 1403 spectrometer, a photomultiplier, a boxcar average, and a computer data acquisition.

Results and Discussion

A. Morphology and Structure. Figure 1 shows the XRD patterns of SBA-15, which were provided by Jilin University to characterize the ordered mesoporous structure. In Figure 1, the XRD patterns show three characteristic diffraction peaks that are indexed to (100), (110), and (200) diffraction, being typical of two-dimensional hexagonal (*p*6*mm*) SBA-15. The nitrogen adsorption and desorption isotherms display type-IV isotherm curves with an H1 hysteresis loop at high relative pressure, indicating the presence of large pores with narrow pore size distribution. The textural data of the materials are summarized as follows: BET surface area, 832.0580 m^2/g; pore diameter, 6−7 nm; and pore volume, 1.26 cm^3/g.

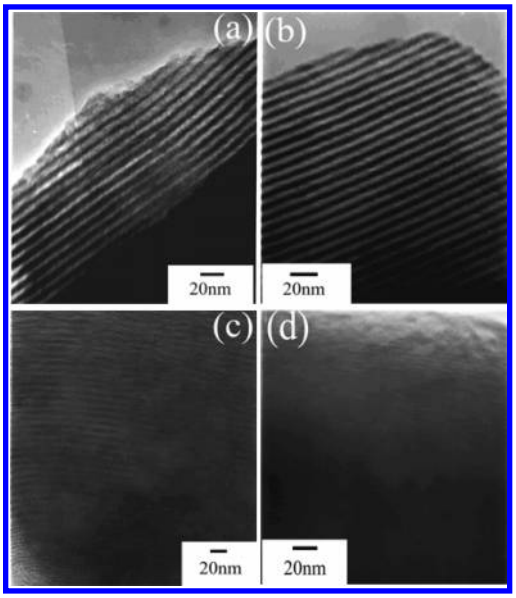

Figure 2. TEM images of SBA-15 (a), modified SBA-15 (b), and samples **A** (c) and **B** (d).

TABLE 1: Variation of the Content of Tb^{3+}, Relative Emission Intensity, Radiative and Nonradiative Transition Rates (Room Temperature) for the $^5D_4$ State, and Fitting Parameters α and E_A According to Equation 1 in the Text

sample	P	A	B
content of theTb^{3+} (mass %)	100	1.74	1.38
relative intensities of $^5D_4$-$^7F_5$	100	8.2	2.6
radiative rate (μs)	1180	910	640
nonradiative rate (μs)	0	760	0
α	6.9	31.3	40.7
E_A (meV)	53.9	91.1	102.9

Figure 2a−d shows, respectively, TEM images of SBA-15, modified SBA-15, and samples **A** and **B**. It can be seen that the average pore diameter of unmodified SBA-15 is 6−7 nm, whereas the diameter of the modified SBA-15 decreases to 4−5 nm. Figure 2c and d demonstrates that the pores are fully filled in samples **A** and **B**. The fillings should be the pure Tb(acac)$_3$phen complexes, which was supported by the results of element analysis. For raw Tb(acac)$_3$phen complexes, the concentrations of C, N, and H were determined to be, respectively, 50.64, 4.50, and 4.92% in weight ratio, which is consistent with the calculated values, 50.95, 4.40, and 4.59%. For byproducts in filtered solution produced by fabricating samples **A** and **B**, they were determined to be 49.24, 4.07, and 4.60%. The similar components between Tb(acac)$_3$phen complexes and byproducts imply that no chemical reaction occurred between Tb(acac)$_3$phen complexes and SBA-15, which indirectly suggests that the fillings were pure Tb(acac)$_3$phen complexes, instead of reacted products. The contents of the Tb^{3+} ions in different samples were obtained by ICP-AES measurement, to be 1.74% in sample **A** and 1.38% in **B**, as listed in Table 1.

Figure 3 shows the FTIR absorption spectra of various samples. As shown in Figure 3, the vibration modes in the unmodified SBA-15 are consistent with those of typical SBA-15 with *p*6*mm* phase. In comparison with the unmodified SBA-15, two additional peaks are observed, at ∼2934 cm^{-1} and ∼1564 cm^{-1}, corresponding to the C−H stretching mode and N−H bending mode in primary ammine, respectively. Besides,

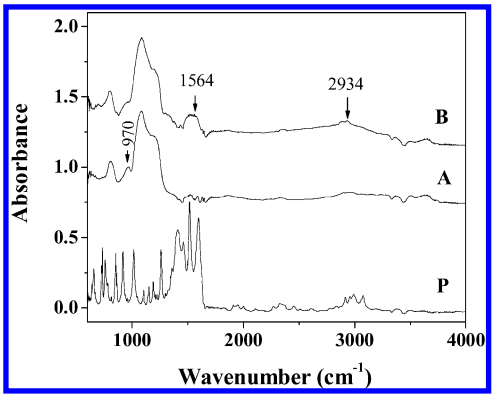

Figure 3. FTIR spectra of samples **P**, **A**, and **B**.

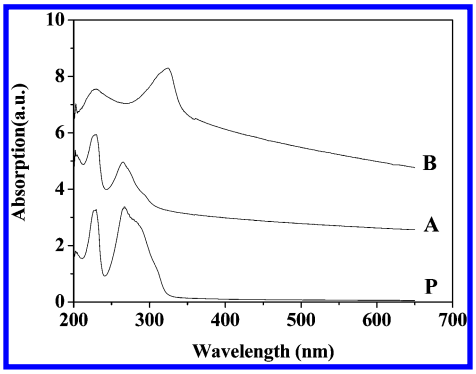

Figure 4. UV−vis absorption spectra of samples **P**, **A**, and **B**.

a weak peak appears at ~970 cm^{-1} in sample **A**, which is assigned to the Si−OH vibration generated by the presence of defect sites, which is characteristic of mesoporous silica.[18] In sample **B**, the intensity of the peak decreases and changes into a shoulder at the same wavenumber. Accordingly, we suggest that $-CH_2NH_2$ groups were grafted onto the surface SBA-15 via reactions between silylating agents (APTES) and OH groups on the channel wall, as follows:

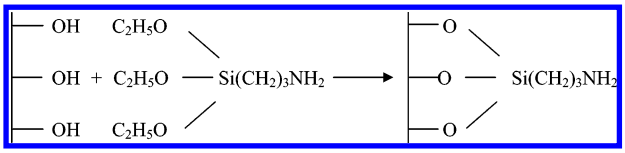

In Figure 3, a number of sharp vibration peaks appear in the range of 800−1200 cm^{-1} and 2880−3124 cm^{-1} for the pure complexes, whereas they do not appear in samples **A** and **B**, which suggests that the pure complexes were actually encapsulated in the pores of the host material but not physically absorbed outside.

UV−vis absorption spectra of different samples are drawn in Figure 4. Two absorption bands located around 228 and 267 nm are observed, corresponding to the $\pi-\pi^*$ transition of the ligands for the pure complexes. In contrast to the pure complexes, the locations of the two bands in sample **A** are nearly the same, which indicates that the pure complexes were dispersed in the channels of unmodified SBA-15. In sample **B**, both absorption bands become broader. In addition, the band at 267 nm red-shifts to 324 nm, which can be attributed to the inducement interaction between NH groups and the complexes, generating a nephelauxetic effect and decreasing the conjugation[19] in the Tb^{3+} complexes.

B. Excitation and Emission Spectra. It is well known that in the RE complexes the energy is transferred from the triplet state of ligands to the center RE ion, which raises the 4*f* electron

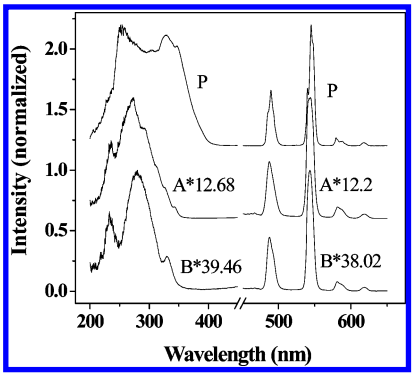

Figure 5. Excitation spectra of the pure complexes and samples **A** and **B** (λ_{em}= 545 nm), and emission spectra of $^5D_4$-^7F_J (J = 3−6) transitions in the pure complexes (λ_{ex} = 254 nm), **A** (λ_{ex} = 272 nm), and **B** (λ_{ex} = 277 nm).

of the ions to excited energy levels. Radiative electronic transitions back to the ground state or to other lower states give off photons. Because of the shielding effect of electrons in the outer shells, inner 4 *f* electronic transitions of the RE ions give rise to a narrow emission band, which is insensitive to the chemical environment. The sensitization pathway in luminescent rare earth complexes generally consists of an initial strong absorption of ultraviolet energy that excites the ligand to the excited singlet (S_1) state, followed by an energy migration via intersystem crossing from the S_1 state to a ligand triplet (T) state. The energy is then nonradiatively transferred from the lowest triplet state of the ligand to a resonance state of a coordinated lanthanide ion, which in turn undergoes a multiphoton relaxation and subsequent emission in the visible region.[20,21]

The excitation and emission spectra of various samples are depicted in Figure 5. It can be seen that a broad excitation band ranging from 200 to 410 nm exists in the excitation spectrum of the pure complexes, which is assigned to the $\pi-\pi^*$ electron transition of the ligands. In samples **A** and **B**, the excitation bands are split into different components and disappear at long wavelengths, which suggests that the ligands environment has been changed. The pure complexes exhibit characteristic emissions of the Tb^{3+} ion with a main peak at 545 nm, corresponding to the $^5D_4$-$^7F_5$ transitions. The emission lines in samples **A** and **B** are the same as those in the pure complexes, but the intensity becomes weaker. The relative fluorescence intensity in different samples ($^5D_4$-$^7F_5$) are listed in the Table 1. By comparing the intensity and the concentration of Tb^{3+} in different samples, we can conclude that the unit mass of the pure complexes in samples **A** and **B** gives stronger luminescence than the pure complexes, implying the improvement of outer luminescence efficiency. Xu et al. also observed a similar phenomenon in the encapsulated Eu^{3+} complexes.[11,12] The unit mass of the pure complexes in sample **B** gives a lower luminescence than that in sample **A**.

On one hand, the excited-state energy for the $\pi-\pi^*$ electron transition of the ligands can be transferred to Tb^{3+}, generating $^5D_4$-^7F_J emissions. On the other hand, it can be transferred into vibration transition energy through electron−phonon coupling. In the pure complexes, a large part of excited-state energy is transferred into vibration transition energy because of strong electron−phonon coupling. For the encapsulated complexes, vibration transition is suppressed because of the existence of a solid bone with boundary of pores. As a consequence, more energy is transferred to Tb^{3+}, leading to the improvement of photoluminescence. In sample **B**, more excited energy is adsorbed by the modified SBA-15 instead of the acac com-

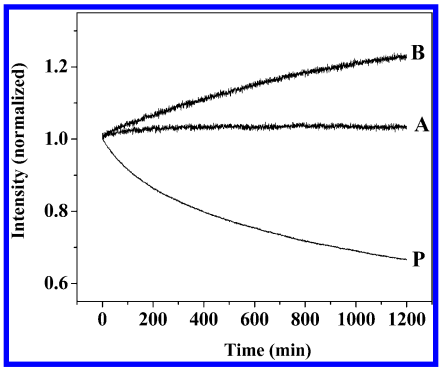

Figure 6. Dependence of emission intensity at 545 nm on irradiation time for various UV lights (λ_{ex} = 272 nm).

plexes, which cannot be effectively transferred to Tb^{3+}. This point is confirmed by the UV−vis absorption spectra, which indicates that the host absorption of SBA-15 in the modified complexes increases compared to that in the unmodified complexes.

C. Photoluminescence Stability. It is well known that the instability of RE complexes under UV irradiation is one of the problems for practical application. In the present work, the dependence of emission intensity on irradiation time was studied in different samples (see Figure 6). As shown, the emission intensity of $^5D_4$-$^7F_5$ in the pure complexes decreases with the increasing exposure time, whereas in sample **A** it is nearly constant. It is more interesting to observe that the intensity in sample **B** even increases with increasing exposure time. Actually, both the unmodified and modified SBA-15 provide a rigid environment for the pure complexes to reduce the energy consumption on vibration of ligands and collision of intermolecular of complexes. And, SBA-15 protects the pure complexes from decomposing under UV irradiation. The intensity enhancement with exposure time in sample **B** can be attributed to optical modification of the surface defects. In the preparation, a large number of surface defects are involved in the inner surface of the pores, which generally act as nonradiative relaxation channels. Under the exposure of UV lights, the defects are modified gradually, causing photoluminescence to increase. Xu et al. also observed the improvement of photostability in the Eu complexes encapsulated in the MCM-41 porous;[11,12] however, the degree of the improvement is not as large as the present results. The reason should be that in the present samples the RE complexes are better distributed into the pores.

D. Temperature Dependence of Emission Intensity. The temperature dependence of fluorescence intensity was measured under the 325-nm excitation in various samples in order to reveal the thermal stability of photoluminescence. Figure 7a and b shows, respectively, the emission spectra at various temperatures in sample **A** and the dependence of emission intensity on temperature in various samples. It can be seen that the emission intensity of $^5D_4$-^7F_J for the Tb^{3+} ion in all of the samples decreases monotonically with increasing temperature in the studied range. In comparison with that in the pure complexes, the emission intensity of $^5D_4$-^7F_J in samples **A** and **B** changes more slowly in the range of 77−157 K, and more rapidly above 157 K. In Figure 7b, the intensity as a function of temperature is well fitted by the well-known thermal activation function[22]

$$I(T) = \frac{I_0}{1 + \alpha e^{-E_A/K_B T}} \quad (1)$$

where I_0 is the emission intensity at 0 K, α is the proportional coefficient, E_A is the thermal activation energy, κ_B is Boltzi-

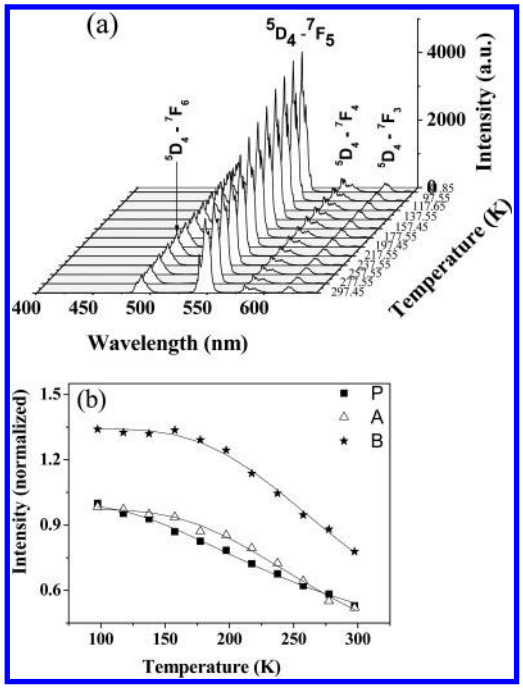

Figure 7. (a) Emission spectra of the pure complexes at different temperatures; (b) dependence of $^5D_4$-$^7F_5$ emission intensity on temperature in samples **P**, **A**, and **B** (λ_{ex} = 325 nm).

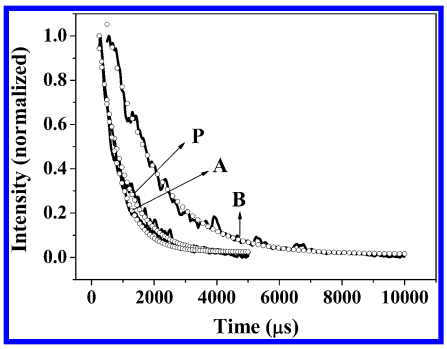

Figure 8. Fluorescent decay curves of the $^5D_4$-$^7F_5$ transitions at 545 nm in various samples (λ_{ex} = 266 nm). The solid lines are experimental data, and the circles are fitting functions.

mann's constant, and T is the absolute temperature. The values of α and E_A obtained by fitting are listed in Table 1. The improved value of E_A in samples **A** and **B** suggests that the photoluminescence is more stable than that in the pure complexes.

E. Dependence of Fluorescence Lifetime on Temperature. Figure 8 shows the fluorescence decay curves of the $^5D_4$-$^7F_5$ transitions for Tb^{3+} ions in various samples. It can be seen that the $^5D_4$-$^7F_5$ transitions all decay exponentially. The exponential lifetimes are deduced to be 834 μs in the pure complexes, 633 μs in sample **A**, and 1528 μs in sample **B**. It is apparent that the lifetime in sample **A** becomes shorter than that in the pure complexes, whereas that in sample **B** becomes longer. The lifetime can be written as

$$\tau = \frac{1}{W_r + W_{nr}} \quad (2)$$

where W_r and W_{nr} are, respectively, the total radiative transition rate of $^5D_4$-Σ^7F_J and the nonradiative relaxation rate. To deduce the radiative and nonradiative rates, the dependence of lifetime on temperature was measured, as shown in Figure 9. It can be observed that the decay time constant of $^5D_4$-$^7F_5$ in samples **P**

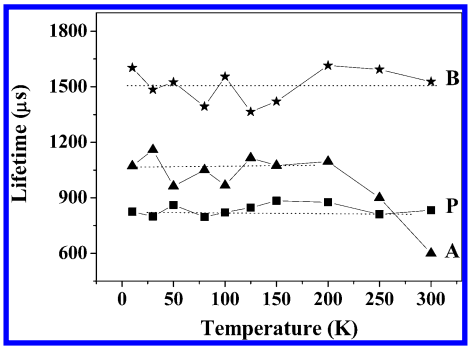

Figure 9. Dependence of fluorescence lifetimes for the $^5D_4$-$^7F_5$ transition on temperature. The fluorescence decay curves are measured under the excitation of the 266-nm light.

and **B** is nearly constant in the studied temperature range. In sample **A**, the lifetime constant of the $^5D_4$-$^7F_5$ transition is nearly constant below 200 K, whereas in the range of 200−300 K the lifetime decreases quickly with increasing temperature. As is well known, the radiative transition rate is almost independent of temperature, whereas the nonradiative relaxation rate depends strongly on temperature and can usually be described by the theory of multiphonon relaxation.[23] At a low enough temperature, the nonradiative relaxation rate is negligible. The radiative relaxation rate is equal to the reverse of lifetime; accordingly, it is deduced to be 1180 μs^{-1}in the pure complexes, 910 μs^{-1} in sample **A**, and 640 μs^{-1} in sample **B**. Then, the nonradiative relaxation rate at room temperature is also determined to be zero in samples **P** and **B** and 760 μs^{-1} in sample **A**. The inner quantum efficiency can be written as

$$\eta_{\text{inner}} = W_r/(W_r + W_{nr}) \tag{3}$$

On the basis of eq 3, the values of η_{inner} in samples **P**, **A**, and **B** are determined to be 100%, 55% and 100%, respectively. η_{inner} in sample **A** decreases in comparison to the pure complexes, whereas that in sample **B** does not change.

The increase of the nonradiative transition rate in sample **A** can be attributed to the influence of the SBA-15 surrounding the complexes. The SBA-15 may adsorb some water on the surface, which generally acts as a luminescence killer, resulting in improved nonradiative relaxation.[24] The decrease of radiative transition rate in sample **A** may be related to the influence of the variation of the refractive index. The radiative transition lifetime can be written as follows

$$\tau_R \approx \frac{1}{f(ED)} \frac{{\lambda_0}^2}{\left[\frac{1}{3}(n^2+2)\right]^2 n} \tag{4}$$

where f(ED) is the oscillator strength for the electronic dipole transition, λ_0 is the wavelength in vacuum, and n is the refractive index of the material. R. S. Meltzer et al. observed that the radiative fluorescence lifetime of Y_2O_3/Eu nanocrystals is dependent not only on the refractive index itself but also on the surrounding medium. They deduced that in nanoparticles n in eq 4 should be substituted by the effective refractive index $n_{\text{eff}} = xn + (1 - x)n_{\text{med}}$, where x is the filling factor showing what fraction of the space is occupied by the nanoparticles and n_{med} is the refractive index of the surrounding media.[25] In the present case, the complexes are surrounded by SBA-15 mesoporous molecule sieves. The values of refractive index are, respectively, 1.4260 for acac[26] and 1.15 for SBA-15.[27] This will lead n_{eff} to be smaller than n, which would induce the increase of radiative lifetime.

Summaries

We encapsulated and characterized the RE complexes Tb(acac)$_3$phen in unmodified and modified mesoporous molecular sieves, SBA-15, which provided a rigid environment for the RE complexes. Their photoluminescence properties including absorption, excitation and emission spectra, fluorescence dynamics, and temperature dependence of emissions were systemically studied. The results demonstrated that in the unmodified and modified SBA-15 the excitation bands assigned to the $\pi-\pi^*$ electron transition of the ligands were split into different components because of decreased symmetry and disappeared at long wavelengths. The temperature dependence of the fluorescence lifetime indicated that the radiative transition rate of $^5D_4$-Σ^7F_J in samples **A** and **B** decreased in comparison to the pure complexes, which originated from the influence of the refractive index of the surrounding media (SBA-15). In sample **A**, the nonradiative transition rate for the $^5D_4$ state became larger at room temperature, leading the inner quantum efficiency to decrease. Anyway, the outer quantum efficiency of photoluminescence in sample **A** became much larger than the pure complexes as well as sample **B**, which was attributed to more efficient energy transfer from the ligands to Tb^{3+}.

In the SBA-15, the photostability of the Tb complexes was improved considerably in comparison to the pure complexes. In the modified sample, it is interesting to observe that the emission intensity increased with the increasing irradiation time, which was attributed to the modification of surface defects under the exposure of ultraviolet light. The thermal stability for the samples encapsulated in SBA-15 was also improved considerably. Overall, the photoluminescence properties of Tb^{3+} complexes encapsulated in SBA-15 were improved considerably in comparison to the pure complexes, which is essentially important for future application of RE complexes in areas of both molecular optical and electrical devices.

Acknowledgment. We are thankful for financial support by National Natural Science Foundation of China (Grants 10374086 and 10504030) and the Talent Youth Foundation of JiLin Province (Grants 20040105).

References and Notes

(1) Lehn, J. M. *Angew. Chem., Int. Ed. Engl.* **1990**, *29*, 1304.
(2) De S'a, G. F.; Malta, O. L.; De Mello Doneg'a, C.; Simas, A. M.; Longo, R. L.; Sata-Cruz, P. A.; Da Silva, E. F., Jr. *Coord. Chem. Rev.* **2000**, *196*, 165.
(3) McGehee, M. D.; Bergstedt, T. B.; Zhang, C.; Saab, A. P.; O'Regan, M. B.; Bazan, G. C.; Srdanov, V. I.; Heeger, A. J. *Adv. Mater.* **1999**, *11*, 1349.
(4) Hu, W.; Matsumura, M.; Wang, M.; Jin, L. *Appl. Phys. Lett.* **2000**, *77*, 26.
(5) Zheng, Y.; Fu, L.; Zhou, Y.; Yu, J.; Yu, Y.; Wang, S.; Zhang, H. *J. Mater. Chem.* **2002**, *12*, 919.
(6) Serra, O. A.; Rosa, I. L. V.; Medeiros, C. L.; Elizabete, M.; Zaniquelli, D. *J. Lumin.* **1994**, *60−61*, 112.
(7) Matthews, L. R.; Knobbe, E. T. *Chem. Mater.* **1993**, *5*, 1697.
(8) Qian, G.; Wang, M.; Wang, M.; Fan, X.; Hong, Z. *J. Mater. Sci. Lett.* **1997**, *16*, 322.
(9) Rosa, I. L. V.; Serra, O. A.; Nassar, E. J. *J. Lumin.* **1997**, *72−74*, 532.
(10) Serra, O. A.; Nassar, E. J.; Zapparoll, G.; Rosa, I. L. V. *J. Alloys Compd.* **1994**, *207−208*, 454.
(11) Xu, Q. H.; Li, L. S.; Li, B.; Xu, R. R. *Microporous Mesoporous Mater.* **2000**, *38*, 351.
(12) Xu, Q. H.; Li, L. S.; Liu, X. S.; Xu, R. R. *Chem. Mater.* **2002**, *14*, 549.
(13) Zhang, M. S.; Yin, W.; Su, Q.; Zhang, H. J. *Mater. Lett.* **2002**, *57*, 940.
(14) Fernandes, A.; Dexpert-Ghys, J.; Gleizes, A.; Galarneau, A.; Brunel, D. *Microporous Mesoporous Mater.* **2005**, *83*, 35.

(15) Zhao, D.; Huo, Q.; Feng, J.; Chmelka, B. F.; Stucky, G. D. *J. Am. Chem. Soc.* **1998**, *120*, 6024.

(16) Yan, B.; Zhang, H. J.; Wang, S. B.; Ni, J. Z. *Mater. Chem. Phys.* **1997**, *51*, 92.

(17) Zemanian, T. S.; Fryxell, G. E.; Liu, J.; Mattigod, S.; Franz, J. A.; Nie, Z. *Langmuir* **2001**, *17*, 8172.

(18) Cheng, Q. L.; Pavlinek, V.; Lengalova, A.; Li, C. Z.; He, Y.; Saha, P. *Microporous Mesoporous Mater.* **2006**, *93*, 263.

(19) Latva, M.; Takalo, H.; Mukkala, V. M.; Matachescu, C.; Rodriguez-Ubis, J. C. *J. Lumin.* **1997**, *75*, 149.

(20) Tanaka, M.; Yamagughi, G.; Shiokawam, J.; Yamanaka, C. *Bull. Chem. Soc. Jpn.* **1970**, *43*, 549.

(21) Haynes, A. V.; Drickamer, H. G. *J. Chem. Phys.* **1982**, *76*, 114.

(22) Li, B. S.; Liu, Y. C.; Zhi, Z. Z.; Shen, D. Z.; Lu, Y. M.; Zhang, J. Y.; Fan, X. W. *J. Cryst. Growth.* **2002**, *240*, 479.

(23) Song, H. W.; Chen, B. J.; Peng, H. S.; Zhang, J. S. *Appl. Phys. Lett.* **2002**, *81*, 1776.

(24) Li, H. R.; Lin, J.; Zhang, H. J.; Fu, L. S.; Geng, Q.; Wang, S. B. *Chem. Mater.* **2002**, *14*, 3651.

(25) Meltzer, R. S.; Feofilov, S. P.; Tissue, B.; Yuan, H. B. *Phys. Rev. B* **1999**, *60*, 14012.

(26) Dean, J. A.; Wei, J. F. *Lange*'s *Handbook of Chemistry*, 2nd ed.; Science Press: Beijing 2003; p 233.

(27) Bartl, M. H.; Boettcher, S. W.; Frindell, K. L.; Stucky, G. D. *Acc. Chem. Res.* **2005**, *38*, 263.